Applied Catalysis B: Environmental 144 (2014) 216–222

Contents lists available at ScienceDirect

Applied Catalysis B: Environmental

journal homepage: www.elsevier.com/locate/apcatb

Preparation of smart nano-engineered electrospun membranes for methanol gas-phase photoxidation

Michele Modesti*, Martina Roso, Carlo Boaretti, Stefano Besco, Denis Hrelja, Paolo Sgarbossa, Alessandra Lorenzetti

University of Padova, Department of Industrial Engineering, Via Marzolo, 9, 35131 Padova, Italy

ARTICLE INFO

Article history:
Received 27 March 2013
Received in revised form 4 July 2013
Accepted 8 July 2013
Available online 17 July 2013

Keywords:
Multistructured membranes
VOCs removal
Nanofibers
Electro-hydrodynamic technologies

ABSTRACT

Nano-engineered membranes obtained by electro-hydrodynamic technologies have been proposed as a good candidate for active filtration. The present work reports some results on the development, production and characterization of three different nanostructured membranes based on: electrospun TiO_2 inorganic nanofibers, nanocomposite structures of polymer nanofibers with TiO_2 embedded nanoparticles and multilayered structures of polymer nanofibers and electrosprayed TiO_2 nanoparticles. Their catalytic activity on volatile organic compounds (VOCs) decomposition has been explored in a photoreactor properly design for this purpose and a comparison among their performance will be extensively discussed. Multilayered membranes showed a complete degradation of methanol in gas phase and the photo-catalytic activity has been found to be affected from the catalyst content and morphology, by means that there is a critical concentration of catalyst over which its increase results on worse photo-oxidation performance. Inorganic TiO_2 based membranes revealed the same activity as the nanocomposite membranes, in terms of methanol reacted per gram of catalyst, but their poor mechanical properties makes them not suitable for a potential scale up.

1. Introduction

In the last decade many efforts have been done in the nanotechnology fields thanks to the awareness that most of major disciplines, from chemistry, physics, medicine to engineering tend to converge at the nanoscale toward some basic structures, principles and tools of investigation. Based on this multidisciplinary perspective, new challenges appear, offering a unimagined tasks for scientific discovery and technological applications.

The development of new solutions in pollution sensing and prevention by using adequate nanostructures with unique properties has gained more interest according to a pressing need for new advanced solutions both for indoor and outdoor pollution. At this regard, polymer nanofiber technology starts its evolution in 90s [1] and is still growing rapidly as the usefulness of nanofibers became apparent in the scientific and business communities [2]. Nanofiber filter media have enabled new levels of filtration and environmental clean up performances in a broad range of applications since they have proven to be a good candidate for promoting a significant increase in filter efficiency and more contaminate holding capacity [3].

According to the United States Environmental Protection Agency (EPA), the concentrations of many VOCs are consistently higher indoors (up to ten times higher) than outdoors. VOCs are emitted by a wide array of products numbering in the thousands (paints and lacquers, paint strippers, cleaning supplies, pesticides, building materials and furnishings, to cite just few examples) and the Indoor Air Quality (IAQ) has become an important community concern due to the increased amount of personal time spent in indoor environment. The ability of organic chemicals to cause health effects varies greatly from those that are highly toxic, to those with no known health effect. Among the methods suggested to improve the indoor air quality, traditional pollution control method such as adsorption by activated carbon merely transfers pollutants from gaseous phase to solid phase [4]. Consequently, advanced oxidation processes (AOP) such as thermal oxidation destruction [5–7] and photocatalytic oxidation (PCO) [8,9] are promising technologies for air purification because the pollutants can be oxidized to H_2O and CO_2.

Within this scenario this work represents an important step within the broad research on the development of an "active" filter media which couple both the physical action, for particulates removal, and chemical action, for VOC decomposition.

Recently, numerous studies have concentrated on the degradation of volatile organic compounds via photocatalysis of various semiconductors. Among the photocatalysts, TiO_2 with anatase

* Corresponding author. Tel.: +39 0498275541.
E-mail address: michele.modesti@unipd.it (M. Modesti).

0926-3373/$ – see front matter © 2013 Elsevier B.V. All rights reserved.
http://dx.doi.org/10.1016/j.apcatb.2013.07.021

phase has been most widely investigated due to its good photocatalytic activity and chemical stability, non-environmental effect and low cost [10]. Looking at the state of the art of PCO in gas phase, the research mainly focus on the the gas-solid heterogeneous photocatalytic oxidation of several chemicals such as CO, acetone, ethanol, organic sulfides, and dimethyl methylphosphonate [11] and also aromatic compounds like benzene, toluene, ethylbenzene and m-xylene [12]. As regards methanol photo-oxidation, metal-modified TiO_2 [13], Ti Silicalite Molecular Sieve [14] as well as titanium(IV)oxide [15] have been tested as a thin film catalyst or as nanoparticles. Moreover, several scientific papers refers to the development of photocatalytic TiO_2 inorganic nanofibers by electrospinning (ES) method [16,17]. To improve the photocatalytic performance of TiO_2, many researchers try to combine TiO_2 fibers with metal, semiconductor or organic materials with the aim of improving charge separation during photocatalysis or increasing the response of TiO_2 to visible light [18]. The photocatalytic performances of electrospun inorganic TiO_2 have been tested for the degradation of organic molecules such as methylene blue and methyl orange [19] while other systems, such as Pt/TiO_2, and WO_3/TiO_2, have been tested, in the form of film deposited within a photoreactor, toward several VOCs degradation in vapor phase [20–23].

Despite the good photocatalytic performances, the well-known trouble with inorganic nanofibers regards their mechanical resistance, which makes the final membrane very hard to handle.

According to this and to the state of art of our knowledge, there are no published papers on the photocatalytic degradation of VOCs, such as methanol, evaluated in gas phase and on polymer based membranes obtained by electrospinning (ES) and electrospraying (EHDA).

In the present study we report the results of the development, characterization and catalytic performances of three different kinds of membranes:

- Membranes based on TiO_2 inorganic electrospun nanofibers (Type1).
- Nanocomposites membranes based on polymer nanofibers and TiO_2 nanoparticles embedded within the organic scaffold (Type2).
- Multilayered membranes based on polymer nanofibers and TiO_2 electrosprayed nanoparticles (Type3).

A comparison among their photocatalytic activity on methanol degradation has been carried out in a properly designed photoreactor and experiments have been run in discontinuous mode.

2. Experimental

2.1. Materials

Poly(vinyl pyrrolidone) (PVP, *Mw* = 1,300,000 g/mol), titanium (IV) isopropoxide ($Ti(OCH(CH_3)_2)_4$), poly(methyl methacrylate-co-methacrylic acid) (PMMAcoMAA, *Mw* = 34,000 g/mol), polyacrilonitrile (PAN, *Mw* = 150,000 g/mol) were all purchased from Sigma–Aldrich, USA, as well as the solvents ethanol, acetic acid (99 wt%), *N*,*N*-dimethylformamide (used as a solvent after dehydration by storage over molecular sieves). Aeroxide® P25, TiO_2 was purchased from Evonik industries.

2.2. Membrane production and characterization

2.2.1. Titanium dioxide nanofibers production

A solution containing 2 mL of titanium(IV) isopropoxide (TIP) and 2 mL of glacial acetic acid was prepared. This solution was added to 4 mL of a 10 wt.% PVP solution in ethanol. The homogeneously mixed colloid was transferred into a 5 ml syringe fitted with a metallic needle of 0.4 mm of inner diameter. The syringe was fixed horizontally on the syringe pump (NE-300 single syringe pump, NewEra Pump System Inc.) and the positive electrode of the high voltage power supply (Gamma High Voltage Inc. (Ormond Beach, FL)), capable of generating voltages up to 60 kV, was clamped to the metal needle tip. The flow rate of polymer solution was kept at 2.5 ml/h, the applied voltage was 12.5 kV and the tip-to-collector distance was kept at 12 cm. All experiments were conducted at room temperature. The obtained nanofiber mats were initially dried for 24 h at 50 °C under vacuum and then calcined in oven at 500 °C in air for 1 h, with a heating rate of 10 °C/min. The temperature of thermal treatment has been chosen in order to get final nanofibers based on TiO_2-anatase crystals phase rather than rutile, according to the literature [19].

Table 1
Process conditions optimized for both electrospinning (ES) and electrospraying (EHDA).

Process	Voltage (kV)	Flow rate (ml/h)	Electrodes distance (cm)	Needle i.d. (mm)
PAN ES	15	2	25	0.4
TiO_2 EHDA	15	8	12	1.2

2.2.2. Nanocomposite membranes preparation

PMMAcoMAA has been chosen because of the presence of –COOH pendent groups, which are able to interact with the –OH groups on the TiO_2 surface under atmospheric conditions. A solution in *N*,*N*-dimethylformamide was prepared at a concentration in polymer of 23% weight by weight and subsequently a concentration of 12% (w/w on the polymer) of Aeroxide® P25, TiO_2 was added as a catalyst. The final suspension was mixed by ultrasonic mixer (VibraCell VC 505 (500 watts), Sonics&Material, Inc.) and then electrospun at a voltage of 17 kV and a 1.5 ml/h flow rate, with a distance electrode-collector of 15 cm.

2.2.3. Multistructured membranes preparation

According to the methodology previously published [24], polyacrylonitrile solutions in *N*,*N*-dimethylformamide were prepared at a concentration of 5% in polymer weight by weight and then electrospun (ES) on a plate collector. After a suitable amount of fibers had been collected, electrospinning was stopped and electrospraying (EHDA) of nanoparticles suspension (TiO_2, 5%, w/w in ethanol, 40 min ultrasonication at 40% amplitude and dispersant agent addition, according to [24]) was performed in order to spread the nanoparticles over the nanofibers surface. The optimized conditions for both processes are shown in Table 1. Subsequently, one more electrospinning stage was carried out to obtain the final membranes. The membranes were stored overnight in a vacuum chamber for drying and solvent stripping. The amount of catalyst has been express in terms of mg of catalyst per cm^2 of membrane surface.

Different concentrations of TiO_2 were tested, 2.56 mg/cm^2, 1.2 mg/cm^2 and 0.69 mg/cm^2, respectively.

2.2.4. Characterization techniques

All the produced membranes were characterized in terms of morphological analysis by Scanning Electron Microscopy (Obducat CamScan MX2500; Cambridge, UK). Further investigation on nanocomposites membranes has been carried by Transmission Electron Microscopy TEM (FEI Tecnai G12) in order to have a better understanding of the TiO_2 nanoparticles dispersion within the nanofibers.

Table 2
Features of the tested membranes.

Membrane type ID	Processing technique	Features	TiO_2 content (mg/cm^2)
Type 1	ES + Pyrolysis	TiO_2 nanofibers	4.24
Type 2	ES	Polymer nanofibers with TiO_2 embedded nanoparticles	2.13
Type 3_0.69	ES/EHDA	2 layers of nanofibers + 1 layer of nanoparticles	0.69
Type 3_1.2	ES/EHDA	2 layers of nanofibers + 1 layer of nanoparticles	1.2
Type 3_2.68	ES/EHDA	2 layers of nanofibers + 1 layer of nanoparticles	2.68

The catalyst content was evaluated by thermogravimetric analysis (Q-600 TA Instruments) and the analysis were performed in alumina pan type, in air, with a heating rate of 20 °C/min.

X-ray Diffraction (XRD) was used for identification of the crystal phases on the inorganic based membranes. Diffraction measurements were carried out in a 2θ angular range of 1.5–60° on a Philips X'Pert PRO diffractometer, working in reflection geometry and equipped with a graphite monochromator on the diffracted beam (CuKa radiation). The scan step size was 0.02° with a measured uncertainty in terms of d-spacings of about 0.05 nm (2 s).

The features of the tested membranes are summarized in Table 2.

2.3. Photocatalytic experiments

The photocatalytic activities of TiO_2 nanofibers, nanocomposite membranes (polymer nanofibers with TiO_2 nanoparticles) and multistructured membranes (polymer nanofibers and TiO_2 electrosprayed nanoparticles) were investigated by a gas-phase analysis, by means of GC–MS, of the degradation of methanol under UV illumination. A proper photoreactor has been designed for this purpose (Fig. 1) and the experimental set up scheme is shown in Fig. 2.

Fig. 1. Photo-reactor designed for lab experiments.

The photocatalytic reactor (Fig. 1) used is a Pyrex tubular reactor (length 370 mm, internal diameter 100 mm, 2780 cm^3 volume). The reactant mixture is flowing from the top to the bottom, throughout 5 membranes (total surface equal to 342 cm^2) placed on a scaffold, which can be easily removed from the inner part of the reactor. The UV source is a commercial 16 W UV Stylo E16 (Light Progress) with a spectral peak centered around 250 nm, put inside the reactor.

As represented in Fig. 2, the inlet gas stream, controlled by a mass flow controller, was continuously bubbling through a saturator containing the organic compound. Before starting experiments, which were performed in discontinuous mode, the batch reactor was flushed with methanol/air mixture at 155 cm^3/min for two hours for conditioning the system. Once the concentration of VOCs was stabilized, the valves of the reactor were closed, the UV lamp was turned on and the concentration of VOCs was recorded with the reaction time throughout the test. Sampled VOCs were injected through a six-port external injection GC valve (6890 Valco Instrument Co., Inc.) with a 2 ml sample loop. The samples were then transferred to a gas chromatograph HP G1800C GCD series II GC/MS whit pure helium as a carrier gas and with a capillary column MEGA (0.32 i.d., 30 m length and 5 μm thickness).

The initial concentration of methanol has been evaluated working on a calibration curve, where the vapour fractions of methanol at different temperatures were evaluated by Rault–Dalton's law

$$y_i P = \gamma_i x_i P_i^{sat}(T) \quad (i = 1, 2, \ldots N) \tag{2.1}$$

where x_i is a liquid-phase mole fraction, y_i is a vapor-phase mole fraction, and P_i^{sat} is the vapor pressure of pure species i at the temperature of the system. Results have been reported as number of mole reacted per gram of catalyst and a calibration curve has been calculated for each product of reaction in order to monitor their concentration during experiments.

All the obtained results, as the mean value on three different runs, were normalized by the catalyst weight and the reacted moles or the molar flow rates per gram of catalyst where calculated.

3. Results and discussions

3.1. Membranes characterization

Inorganic TiO_2 based membranes were characterized by SEM analysis both before and after heat treatment. Looking at the

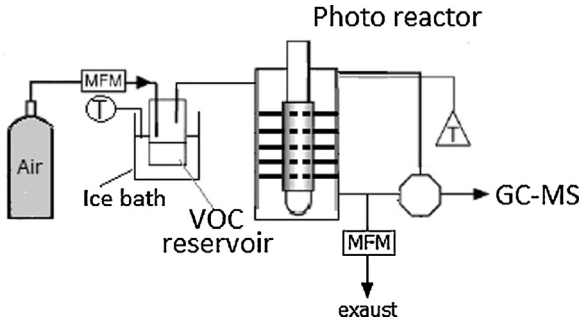

Fig. 2. Schematic diagram of catalyst performance test system.

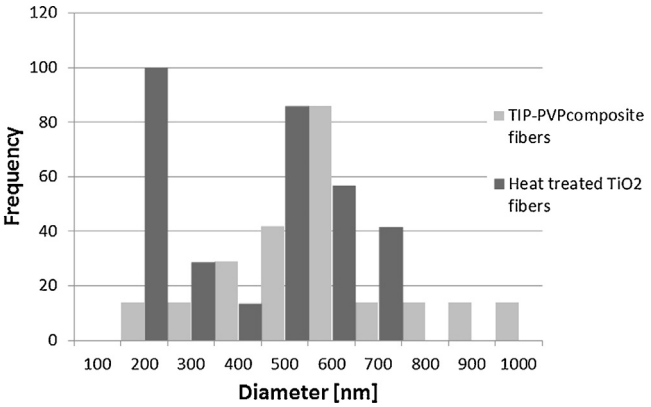

Fig. 3. Distribution of the fibers diameters of inorganic based membranes (TiO_2) before and after heat treatment.

histogram of the distribution of the fibers diameters (measured by ImageJ), Fig. 3, it has been found a variation from a Gaussian distribution curve (mean diameter roughly 607 ± 220 nm) of the PVP–TIP electrospun sample, to a bimodal curve of the TiO_2 calcined sample, where two mean values can be depicted, 200 ± 100 nm and 500 ± 100 nm, respectively. The average diameter of the heat-treated fibers was smaller than that of the as-spun fibers due the shrinkage caused by loss of ethanol, degradation of PVP, decomposition of titanium proproxide, and the succeeding sintering. As regards the morphology, TiO_2 nanofibers after sintering appeared beads free, smooth and compact as shown in micrograph of Fig. 4. Moreover, TiO_2 crystallographic structure, evaluated by XRD pattern, showed diffraction peaks at 25.38 and 48.08, that means the fibers had a pure anatase phase with tetragonal structure. It is important to note that the diffraction peak at $2\theta = 20.98$ [23], which corresponds to the crystalline phase of PVP, has been not revealed in the tested samples. This observation was in good correlation with the results of the thermogravimetric analysis, wherein there was no observed loss in mass above 500 °C.

Nanocomposite membrane based on PMMAcoMAA electrospun nanofibers with TiO_2 embedded nanoparticles were characterized in terms of surface morphologies and fiber diameters by scanning electron microscopy. Fig. 5 show a micrograph of the nanocomposite membrane recorded as back-scattered image, and TiO_2 clusters are clearly visible. Mean fibers diameter was found to be 430 ± 130 nm. Looking at the detail of the single nanofiber in Fig. 5, it has been showed that nanoparticles were present both over the surface and partially embedded inside the bulk structure

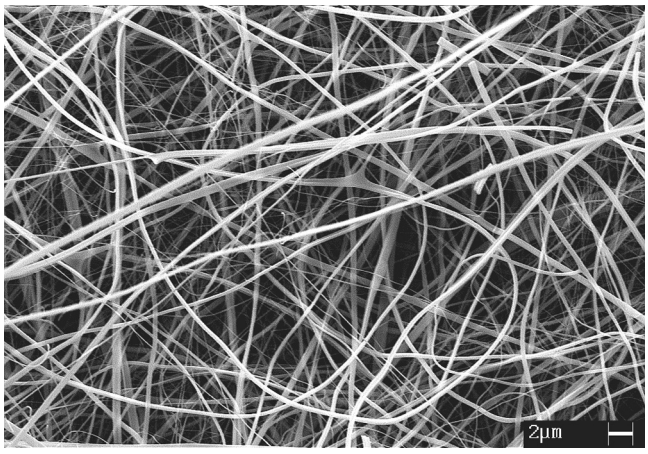

Fig. 4. SEM micrograph of TiO_2 inorganic based membrane after heat treatment.

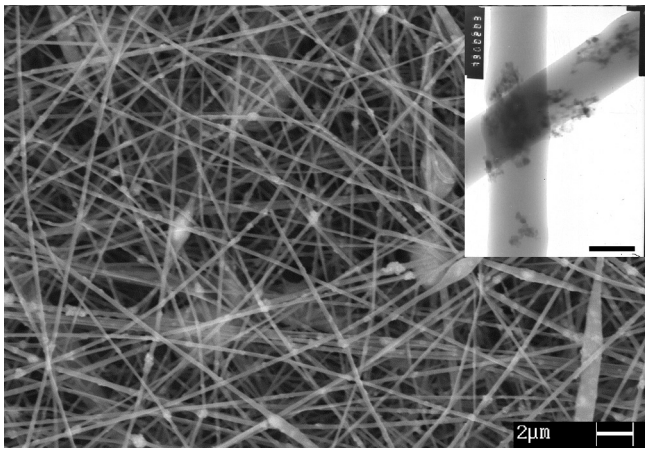

Fig. 5. SEM micrograph of nanocomposite membrane with a detail of the nanofibers by TEM (bar scale 260 nm).

of nanofibers forming clusters. This distribution affected the performance of the membranes as it will be discuss later.

Multistructured membranes based on multi-layered structure (PAN electrospun nanofibers and TiO_2 electrosprayed nanoparticles) showed a mean thickness of 270 ± 20 μm, and mean electrospun fiber diameter of 400 ± 70 nm. The morphology and distribution of TiO_2 nanoparticles over the nanofibers surface has been found to be a function of the electrosprayed amount. At this regards, samples with a TiO_2 content of 2.56 mg/cm^2 reveals the formation of a continuous layer of TiO_2 big clusters which cover all the electrospun web, as shown in Fig. 6a. The electrospun matrix is completely clogged, and this situation affects the effective performance of the membranes themselves. Decreasing the deposition to 1.2 mg/cm^2, the obtained morphology is still based on clusters which partially block the pores among nanofibers (Fig. 6b). The best deposition and morphology has been obtained for samples with a TiO_2 mean content of 0.69 mg/cm^2, where the nanoparticles are uniformly spread over the nanofibers surface as shown in Fig. 6c. The thermogravimetric analysis (TGA) performed on the multistructured membranes, before and after use in catalytic experiments (discontinuous mode), has been useful for evaluating the stability of the membranes and for verifying the amount of exhaust TiO_2. From the thermograms (not reported here, for the sake of brevity) it can be depicted that the residual weight %, which is representative of the only catalyst content, was ranging between 62.5% and 60%, before and after use, respectively. These values and their small variation, allowed the assumption that the catalyst content remained almost constant for all the tested samples. This reflects the stability of TiO_2 which adhered to the nanofibers surface thanks to Van der Waals forces which have been demonstrated [25] to have a strong effect on its microscopic and macroscopic behavior, leading to agglomeration and adhesion to the surface.

3.2. Photocatalytic activity

Our purpose was to compare the effect of catalyst morphology and assemblies on the photocatalytic performances of the whole membranes. According to the experimental setup previously described in Fig. 4, the photocatalytic degradation of methanol has been studied in discontinuous mode for all the nanostructured membranes, and experiments were replicated on three sets of each membrane type, for statistical significance.

Fig. 7 reports the comparison of methanol photo-degradation during the experiment time (discontinuous mode) of all the nanostructured membranes, that is TiO_2 nanofibers based membrane (Type 1), nanocomposite based membrane (Type 2) and

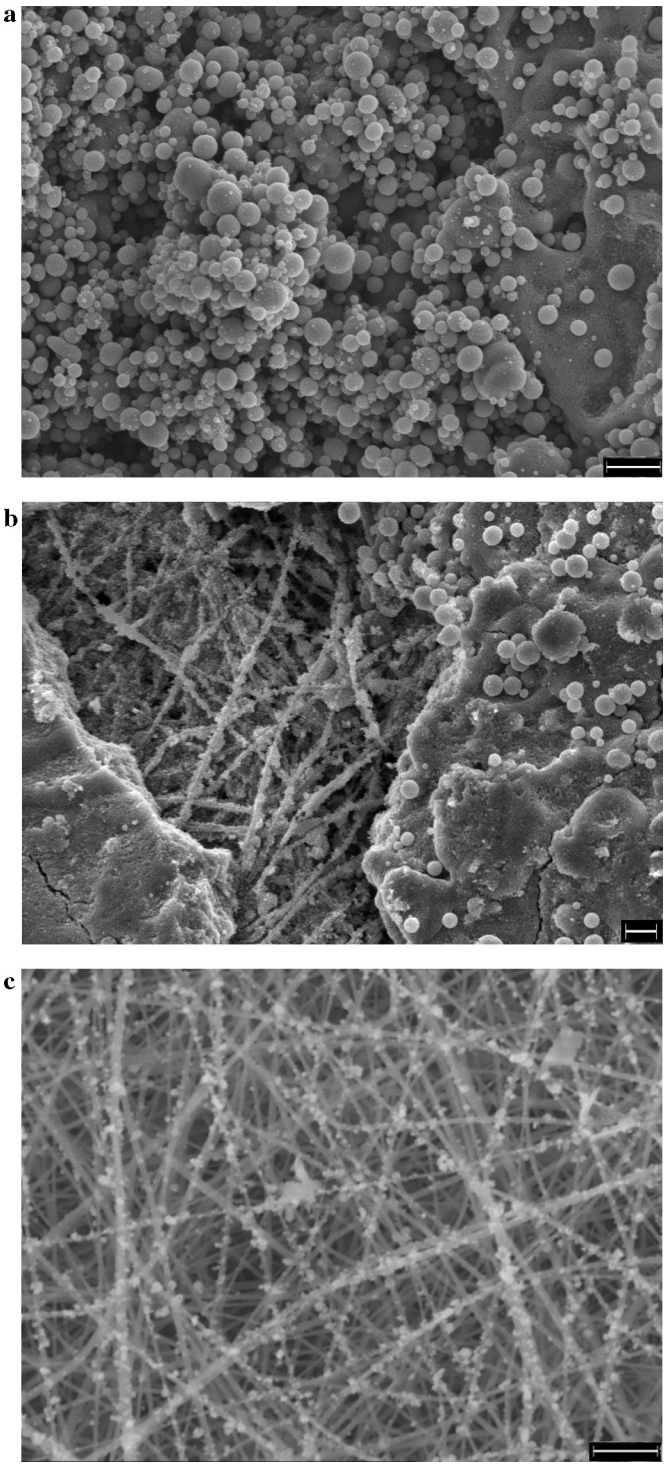

Fig. 6. SEM micrographs of multistructured membranes with different TiO_2 content (a) 2.61 mg/cm^2 (bar scale 5 μm); (b) 1.61 mg/cm^2 (bar scale 3 μm) (c) 0.69 mg/cm^2 (bar scale 5 μm).

multistructured membranes (Type 3, with different catalyst content) with respect the initial concentration of methanol, that is about $y_{0,CH_3OH} = 1350$ppm. All the data have been normalized on the catalyst content (the catalytic surface area being equal) and more in details results have been expressed as the number of moles of methanol reacted per grams of catalyst. Despite the final conversion of $X = 74\%$ obtained with membrane Type 1, with respect to the conversion of $X = 30\%$ on membrane Type 2, Fig. 7 showed clearly that a different conversion depends just on the catalyst content

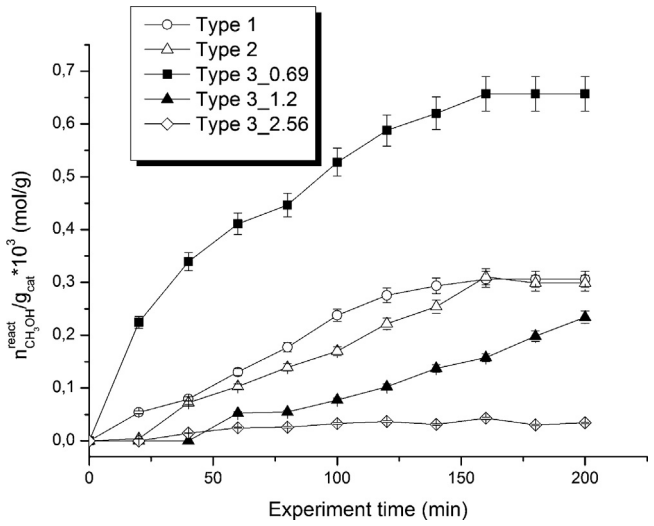

Fig. 7. Methanol moles reacted per g catalyst on inorganic based membrane (Type 1), nanocomposite membrane (Type 2), and on multistructured membrane (Type 3) with different concentrations of catalyst: -■- refers to 0.69 g/cm^2 TiO_2; -▲- refers to 1.269 g/cm^2 TiO_2; -◇- refers to 2.56 g/cm^2 TiO_2 with $y_{0,CH_3OH} = 1350$ppm.

itself. Apparently, for membrane Type 1 and Type 2, the catalyst morphology did not affect the final conversion. Within nanocomposites membrane Type 2 the catalyst was partially spread over the nanofibers surface and partially embedded into the nanofibers, as previously shown in Fig. 5, and it has been hypothesized that the UV-light activation involve just the surface facing catalyst, limiting the performance of the nanocomposite membrane. Furthermore, one reason to explain the obtained results was that the photocatalytic activity of inorganic nanofibers mainly occurred on the nanofibers surface, because of the photo-shielding effect, so that the whole the TiO_2 content was not exploited at all.

Fig. 8 shows the product distribution on multistructured membrane, Type 3_0.69, in terms of concentration–time curve for methanol, and production % for both the intermediate of reaction and CO_2. The methanol concentration in the permeate, that is the concentration at the outlet of the photocatalytic membrane reactor, was reduced to approximately 0 ppm, after a time $t = 160$ min. On the other hand, the approximate concentrations of CO_2 increased from the feed concentration of 450 ppm, contained in the compressed air cylinder, to 880 ppm. It has been also reported the formation of methyl formate as intermediate of

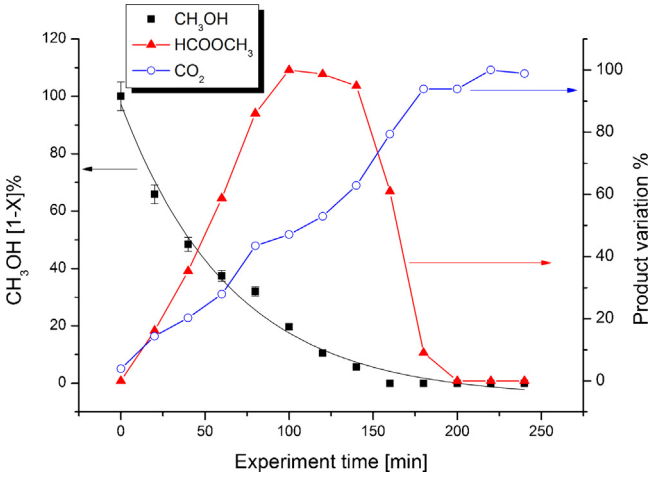

Fig. 8. Methanol photoxidation versus experiment time ($y_0 = 1350$ ppm). CO_2 concentration trend and $HCOOCH_3$ variation % (secondary axis).

reaction which presents a maximum concentration at $t = 100$ min. Methyl formate has been previously reported [14,26] as intermediate of reaction and it could be resulted from the esterification reaction between methanol and formic acid intermediates formed by oxidation of formaldehyde, which has not been detected during run experiments. It has been hypothesized that the degradation of methanol to CO_2 and formation of methylformate occurs in parallel reaction paths. Since the formation of methyl formate is strongly dependent on residual methanol concentration, once the latter was removed from the reaction environment, its concentration was reduced to zero and it was further oxidized to CO_2. Nevertheless, there are other two plausible routes of the formation of methyl formate in oxidation of methanol: (1) condensation of methoxides with formaldehyde to form hemiacetal intermediates (CH_3OCH_2O), which were then dehydrogenated to methyl formate [27], and dimerization of formaldehyde via Tishchenko-type reaction.

According to the majority of publications [13,28], in photocatalysis on n-type semiconductors, organic molecules are oxidatively degraded by direct hole transfer reaction (Eqs. (3.1)–(3.6)), or by products formed by these holes (e.g. OH radicals), indirect hole transfer reaction (Eqs. (3.7)–(3.10)). In the latter reactions, •OH can react with organic substances by hydroxylation through •OH addition onto the organic molecule, followed by further oxidation. However, there was much debate with respect to the reactive active species which played a decisive role during photocatalytic degradation. A few studies demonstrated that $O_2^{\bullet-}$ could be also the major oxidant in photocatalytic reactions [14]. Nevertheless, irrespective of the radical species which initiate the PCO reactions, each oxidation step may proceed on the photocatalyst surface either by the direct interaction of the adsorbed organic species with valence band holes, h^+_{VB}, or by an indirect path involving hydroxyl radical attack [13]. In particular the HCO + CH_3O radical coupling path and the H-transfer step followed by formaldehyde dimerization, is the most validated hypothesis for methylformate generation [14,29].

$$TiO_2 + h\nu \rightarrow e^-_{CB} + h^+_{VB} \quad (3.1)$$

$$CH_3OH(ads) + h^+_{VB} \rightarrow {}^\bullet CH_2OH(ads) + H^+ \quad (3.2)$$

$${}^\bullet CH_2OH(ads) \rightarrow CH_2O + H^+ + e^- \quad (3.3)$$

$${}^\bullet CH_2O(g) + 2O(a) \rightarrow {}^\bullet CHO(g) \rightarrow HO^\bullet_2 \quad (3.4)$$

$${}^\bullet CHO(g) + 2O(a) \rightarrow CO(g) + HO^\bullet_2 \quad (3.5)$$

$$CO(g) + HO^\bullet_2 \rightarrow CO_2(g) + HO^\bullet \quad (3.6)$$

$$H_2O + h^+_{VB} \rightarrow {}^\bullet OH + H^+ \quad (3.7)$$

$$CH_3OH + {}^\bullet OH \rightarrow {}^\bullet CH_2OH + H_2O \quad (3.8)$$

$${}^\bullet CH_2OH + {}^\bullet OH \rightarrow CH_2O + H_2 \quad (3.9)$$

$$CH_2O(g) + 2O(a) \rightarrow CO_2(g) + H_2O \quad (3.10)$$

The effect of nanostructured morphology, being equal other conditions, can be depicted from the results reported in Fig. 7: the number of reacted moles per gram of catalyst, at $t = 160$ min are roughly the same for both membrane Type 1 and Type 2 and are almost half the values for membrane Type 3_0.69, where moles of methanol reacted per g TiO_2 at $t = 160$ are $n = 6.82 \times 10^{-4}$. Hence, the photo-degradation results, wherein membrane Type 3 shows the best performance, has been hypothesized to be related to distribution of the catalyst on the nanofibers. At this regards, the catalyst electrosprayed on multistructured membranes, revealed uniform distribution and the ability of the UV light to activate all the TiO_2 nanoparticles.

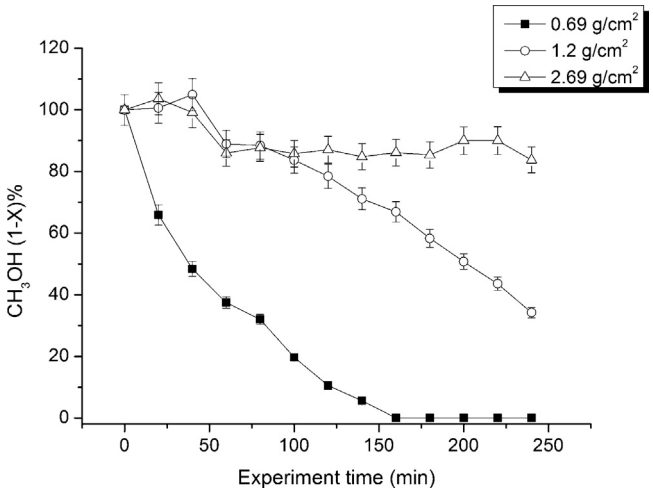

Fig. 9. Methanol photo-oxidation curves parametric on catalyst content (discontinuous mode). $y_{0,CH_3OH} = 1350$ppm.

Inorganic membranes Type 1 have shown good results but they have poor mechanical properties that make them very fragile and very difficult to handle. Because of this and because of the best performance obtained on multi-structured membranes Type 3, further experiments were carried out on the latter.

3.3. Effect of catalyst content

As previously mentioned, in order to evaluate the effect of the catalyst morphology three different concentrations of catalyst have been tested. Fig. 9 shows the time course of the conversion of methanol, the curves being parametric on TiO_2 content. The photo-oxidation at $t = 240$ min grows up from 16% to 65% to 100% as the catalyst content decrease from 2.61 g/cm^2 to 1.2 and 0.69 g/cm^2, respectively. Despite a lower content of catalyst, the photocatalytic performance on the multistructured membranes with low catalyst content are definitely better than the others, and this behavior can be explained looking the number of mole of methanol reacted per gram of catalyst, as shown in Fig. 7. It can be observed that the reacted moles of methanol decrease as the TiO_2 content increase. As previously mentioned, on membrane Type3_2.61 the final morphology shown in Fig. 8a revealed the formation of a continuous filme over the nanofibers surface. This condition has a double effect: first is not possible to exploit the high surface area of nanofibers which represent, in this case, just a substrate; second, once the TiO_2 film was formed on the surface of the electrospun membranes, UV light is not able to penetrate into the whole TiO_2 layer because of the typical photo-shielding, that is, photocatalytic activity enhances with photocatalyst loading until the catalyst layer becomes too saturated for UV light to penetrate. At the saturation point, the generation of electron–hole pairs is significantly reduced [30]. Moving toward a lower concentration, the morphology sensitively changed and a proper photo-activation of the catalyst has been achieved.

Another aspect observed from batch experiments, is the increased photocatalytic efficiency, especially for the membrane Type3_0.69, after the first run, that is, the best performance of multistructured membranes are achieved from the second experiment run performed using the same set of membranes (Table 3). This trend is still not explained at all, and the ongoing work will give a better understanding of the involved mechanisms. However, it has

Table 3
Photoxidation of methanol as a function of catalyst content and experiment run.

Membrane type	N° run	TiO_2 content (g)	Photoxidation % di CH_3OH	CH_3OH reacted (mmol/g)
Type3_2.64	1	0.8780	18.85	0.0468
Type3_1.2	1	0.4122	21.96	0.1380
Type3_1.2	2	0.4122	65.77	0.3124
Type3_0.69	1	0.2365	31.91	0.2306
Type3_0.69	2	0.2365	100	0.8144
Type3_0.69	3	0.2365	100	0.8092

been hypothesized that for this specific pollutant, the controlling step of reaction is the adsorption of methanol on the catalyst surface and the production of electron–hole pairs by near-UV irradiation, followed by hydroxyl radicals formation:

$$CH_3OH_{gas} \rightarrow CH_3OH_{ads} \quad (3.15)$$

Consequently it could be necessary a longer time to achieve this equilibrium.

4. Conclusions

Three different types of photocatalytic membrane were produced, characterized and tested on the degradation of methanol in gas-phase. Inorganic membrane based on TiO_2 nanofibers showed a good performance (conversion of 80%, in batch mode) but because of their poor mechanical properties it has been chosen to move to other nanostructured membranes. Nanocomposite membranes, wherein TiO_2 nanoparticles are embedded in the solution before electrospinning, report a conversion of methanol of 40%, while a complete degradation has been achieved by multistructured membranes based on polymer nanofibers and TiO_2 nanoparticles electrosprayed on their surface. Different concentrations of catalyst were tested and it has been depicted that there is a threshold limit over which the typical photo-shielding take place and this affect the final performance. Moreover the TiO_2 film formation, reported for higher TiO_2 content, does not allow to exploit the high surface area of the electrospun scaffold. Any evaluation of newly developed photocatalysts must be carefully done in order to clearly distinguish the rate limiting step within the observed global kinetics. This is very important especially for supported catalysts for which restrictions to mass transport phenomena must be taken into account.

Acknowledgement

This work was supported by research funding of University of Padova (PRAT 2008 CPDA083825).

References

[1] S. Ramakrishna, K. Fujihara, An Introduction to Electrospinning and Nanofibers, World Scientific Publishing Co., Pte. Ltd., 2005.
[2] M. Modesti, A. Lorenzetti, M. Roso, American Scientific Publisher 17 (2011) 231–312.
[3] W.W.F. Leung, C.H. Hung, P.T. Yuen, Separation and Purification Technology 71 (2010) 30–37.
[4] S. Wang, H.M. Ang, M.O. Tade, Environment International 33 (2007) 694–705.
[5] H. Drysys, Filtration and Separation 34 (1997) 324–329.
[6] K. Everaert, J. Baeyens, Journal of Hazardous Materials 109 (2004) 113–139.
[7] S.E. Roark, J. Cabrera-Fonseca, M.C. Milazzo, J.H. White, J.D. Wander, Journal of Environmental Engineering ASCE 130 (2004) 329–337.
[8] J. Zhao, X.D. Yang, Building and Environment 38 (2003) 645–654.
[9] O. Carp, C.L. Huisman, A. Reller, Progress in Solid State Chemistry 32 (2004) 33–177.
[10] S.J. Doh, C. Kim, S.G. Lee, S.J. Lee, H. Kim, Journal of Hazardous Materials 154 (2008) 118–127.
[11] A.V. Vorontsov, D.V. Kozlov, P.G. Smirniotis, V.N. Parmon, Kinetics and Catalysis 46 (2005) 422–436.
[12] C.A. Korologos, C.J. Philippopoulos, S.G. Poulopoulos, Atmospheric Environment 45 (2011) 7089–7095.
[13] G.L. Chiarello, D. Ferri, E. Selli, Journal of Catalysis 280 (2011) 168–177.
[14] Y.H. Yeom, H. Frei, Journal of Physical Chemistry A 105 (2001) 5334–5339.
[15] H. Kominami, H. Sugahara, K. Hashimoto, Catalysis Communications 11 (2010) 426–429.
[16] M. Srujan, S.P. Ahrenkiel, Journal of Nanomaterials 2012 (2012) 1–6, Article ID 902491.
[17] Y. Wang, J. Zhang, L. Liu, C. Zhu, X. Liu, Q. Su, Materials Letters 75 (2012) 95–98.
[18] M.X. Zhang, H. Pu, S. Nishimoto, T. Murakami, A. Fujishima, Journal of Colloid and Interface Science 362 (2011) 188–193.
[19] A.K. Alves, F.A. Berutti, F.J. Clemens, T. Graule, C.P. Bergmann, Materials Research Bulletin 44 (2009) 312–317.
[20] V. Keller, P. Bernhardt, F. Garin, Journal of Catalysis 215 (2003) 129–138.
[21] K. Demeestere, A. De Visscher, J. Dewulf, M. Van Leeuwen, H. Van Langenhove, Applied Catalysis B 54 (2004) 261–274.
[22] Q.J. Geng, X.K. Wang, S.F. Tang, Biomedical and Environmental Sciences 21 (2008) 118–123.
[23] B. Ding, C. Kim, H. Kim, M. Seo, S. Park, Fibers and Polymers 5 (2004) 105.
[24] M. Roso, S. Sundarrajan, D. Pliszka, S. Ramakrishna, M. Modesti, Nanotechnology 19 (2008) 285707–285712.
[25] J.P.K. Seville, C.D. Willett, P.C. Knight, Powder Technology 113 (2000) 261–268.
[26] E. Sahle-Demessie, C.B. Almquist, S.C. Sehker, Water, Air, and Soil Pollution 8 (2008) 297–309.
[27] C. Louis, J.M. Tatibouët, M. Che, Journal of Catalysis 109 (1988) 354.
[28] S.B. Sadale, K. Noda, K. Kobayashi, H. Yamada, K. Matsushige, Thin Solid Films 520 (2012) 3847.
[29] J. Lichtenberger, D. Lee, E. Iglesia, Physical Chemistry Chemical Physics 9 (2007) 4902.
[30] M.N. Chong, B. Jin, C.W.K. Chow, C. Saint, Water Research 44 (2010) 2997.